

The ortho and para fractions of molecular hydrogen in protostellar outflows and Herbig-Haro objects

Michael D. Smith¹, Christopher J. Davis², and Alain Lioure³

¹ Astronomisches Institut, Universität Würzburg, Am Hubland, D-97074 Würzburg, Germany

² Dublin Institute for Advanced Studies, School of Cosmic Physics, 5 Merrion Square, Dublin 2, Ireland

³CEA / Bruyères-le-Châtel, Service PTN, BP12, F-91690 Bruyères-le-Châtel, France

(e-mail: smith@astro.uni-wuerzburg.de, cdavis@cp.dias.ie)

Received 7 March 1997 / Accepted 1 July 1997

Abstract. Hydrogen molecules exist in two forms, according to the alignment of the nuclear spins. We present an accurate method for extracting the distributions of the two forms from three K-band infrared transitions. Images of the 1-0 S(0), S(1) and S(2) emission lines yield the ortho and para spatial distributions with negligible extinction and model dependence. The ortho-para ratio from individual pointings to various Herbig-Haro outflows are (re-)calculated using our analytical approach. All accurate determinations yield a value between 2.5 and 3.0. The vibrational temperature remains in the range 2000-2500 K although rotational temperatures vary between 1100-2100 K.

Applied to new data for OMC-1, we find no strong evidence for spatial variations in the ortho/para ratio (3.0 ± 0.4) on all scales down to $1''$. The vibrationally-excited molecules have either (1) not been modified since their formation in a warm state or (2) have reached equilibrium through conversions within a warm state. Collisional excitation to the first vibrational level dominates, with no fluorescent component. We suggest that collisions with atomic hydrogen in the warm shock layers converts the ortho-para ratio to 3 locally.

We also find strong evidence for spatial variations in the rotational excitation in OMC-1: the rotational temperature increases from east to west.

Key words: ISM: OMC 1 – ISM: jets and outflows – ISM: molecules – ISM: kinematics and dynamics – infrared: molecular processes – ISM: lines

1. Introduction

At the moment of formation, molecular hydrogen can join one of two denominations: ortho (aligned nuclear spins) or para (opposed nuclear spins). The ortho-para ratio, ϕ , based on the statistical weights of the nuclear spins is 3:1. This is the expected membership ratio when the H_2 has formed on grains at high

temperatures and has avoided subsequent conversion. The ratio can be lowered through conversion on the grains (eg. 1.8, Black & van Dishoeck 1987) or even increased through conversion in the gas phase: thermal collisions with protons or H atoms at low densities yield an equilibrium ratio of $9 \exp(-170 \text{ K}/T)$ (eg. Flower & Watt 1984, Martin, Schwarz & Mandy 1996). Already-published data for the three lines exist for a few single pointings in shock-excited objects. These yield values close to 3:1 (see Sect. 3). However, in photon-dominated regions ratios below 2:1 have been measured (Hasegawa et al 1987, Ramsay et al 1993), consistent with conditions of thermodynamic equilibrium below temperatures of $\sim 100 \text{ K}$. Hence, ϕ can place constraints on the constituents and processes of importance in molecular clouds. Here, we present a method for calculating ϕ and apply it to HH objects. We then present the distribution of ϕ in the OMC-1 bipolar outflow.

The main spectroscopic data obtained here are Fabry-Perot images (from IRAC2 on the ESO 2.2m telescope) in the 1-0 S(0), S(1) and S(2) transitions for the OMC-1 outflow. Also obtained were 2-1 S(1) and 2-1 S(3) images though generally only the brighter nebulous regions near the outflow source were detected. The energy levels of the 1-0 S(0), S(1) and S(2) lines at 6471 K, 6951 K & 7584 K, lie close together - a disadvantage for excitation studies. However, this is balanced by the advantage that the lines are all strong and accurately measurable. Also, a single excitation temperature can be assumed to describe the gas (i.e. the same gas produces all three lines, see Sect. 3). This means that the second piece of information inherent in the two line ratios, ϕ , can be accurately extracted. Moreover, we show in Sect. 3 that the small wavelength separations and the particular order in the spectrum combine to all but exclude differential extinction as a confusing factor.

Recent developments in near infrared detector technology have made mapping of OMC-1 in different lines possible. Many H_2 lines fall in the K-band and a thorough study of those lines can yield considerable information about the physical conditions in these regions. The 1-0 S(2) line has not been imaged before. It is in a spectral region of relatively poor atmospheric transparency

and with the 1-0 S(1) always stronger, there has been no desire to map it. Nevertheless, concurrent equivalent data have been obtained via long-slit spectroscopy by McCaughrean and Mac Low (1997)).

The OMC-1 outflow is situated in one of the best studied star-forming regions (Genzel & Stutzki 1989). It is a prodigious outflow from a high mass protostar, very bright in the infrared lines of molecular hydrogen, although enshrouded in a dense part of the Orion Molecular Cloud (Beckwith et al. 1978). It is hoped that by understanding how the outflow was generated, we can come to terms with this critical star formation phase. Recent infrared and theoretical studies have concentrated on two problem areas: (1) the dynamics which could produce the ‘bullets’ (see below) and (2) the physical processes which excite and accelerate the H₂ without destroying it (Smith 1991; Draine & McKee 1993). Here we employ new near infrared data to explore the basic issues of how the H₂ is formed, modified and excited.

On the dynamical side, Allen & Burton (1992) identified a series of bow shocks in the region north west of IRC2 (Axon & Taylor 1984) as parts of finger-like structures, and claimed that they are due to the ejection of bullets from the center of the exciting region. McCaughrean & Mac Low (1997) have identified a long finger to the south-east of IRC2. Stone et al. (1995) interpreted these data in terms of a fragmenting wind. Another debate concerns the innermost region, close to IRC2. Recent high resolution velocity mapping by Sugai et al. (1995) suggest that a thin shell is interacting with the surrounding cold and static molecular gas.

Near-infrared spectroscopy of OMC-1 has revealed two disturbing facts. First, the molecules appear to be moving extremely quickly, since H₂ line widths approaching ~ 180 km s⁻¹ have been measured (Brand et al.; Tedds et al 1994). There is considerable evidence that the gas in OMC-1 is collisionally excited within shock fronts (Brand et al 1988). However, standard magnetohydrodynamic shocks can only accelerate molecules to speeds of ~ 25 km s⁻¹ (J-type shock) or ~ 50 km s⁻¹ (C-type shock, see Draine & McKee 1993). A possible solution lies in the presence of low Alfvén-speed ‘shock absorbers’ (Smith et al. 1991b) in which the magnetic field ahead of the shock is pre-compressed before being overtaken by the shock. This mechanism permits H₂ excitation (without dissociation) in faster shocks, and so the acceleration to higher velocities.

Secondly, the H₂ excitation in OMC-1, as measured by the temperature of gas required to produce a given ratio of line strengths, is strangely constant in space (Brand et al 1989a). However, Smith (1991a) has shown how a large number of arcsecond-sized curved shocks, or mini-bow shocks, could produce the uniform line ratios. Indeed Smith is also able to account for the observed dependence of excitation temperature on the upper energy levels of the particular transitions. Other possible explanations for this apparently uniform excitation distribution include the shock-dissipation of supersonic turbulence (Davis & Smith 1996) and ‘dry J-shocks’ (Brand et al 1988), although recent ISO observations of abundant H₂O in some out-

Table 1. Fabry-Pérot settings and order sorting filters used

	FP wavelength setting (μm)	Blocking filter wavelength (μm)	$\Delta\lambda/\lambda$ (%)
1-0 S(0)	2.2230	2.216	3.3
Continuum	2.2280	2.216	3.3
1-0 S(1)	2.1217	2.121	3.9
Continuum	2.1286	2.121	3.9
1-0 S(2)	2.0330	2.058	1.7
Continuum	2.0372	2.058	1.7
2-1 S(1)	2.2470	2.216	3.3
Continuum	2.2400	2.216	3.3
2-1 S(3)	2.0727	2.058	1.7
Continuum	2.0765	2.058	1.7

flows (Liseau et al 1996) has cast doubt on the validity of this second model.

In this paper, we now take the OMC-1 puzzle one stage further by posing the question: which shocks are consistent with the ortho-H₂/para-H₂ fractions?

Excitation images may be used to illustrate the spatial distributions of rotational and vibrational excitation temperatures. This has previously been achieved for L 1448 (Davis & Smith 1995) and Cepheus E (Eisloffel et al 1996). Along with the strong 1-0 S(1) line, lines from higher vibrational levels allow the excitation temperature to be derived. This is despite the relative weakness of the measured 2-1 S(1) and 3-2 S(3) lines. The neighbouring lines discussed in this paper do not in principle allow the excitation temperature to be accurately derived. However, as will be seen, the constant ortho-para ratio derived from the same data implies that the excitation temperature can indeed be reliably extracted. Image display of such ratio distributions is hampered by the inevitable inaccuracies in regions of low intensity (for intensity images this is of course no problem). Consequently, here we will display the excitation and ortho-para ratio along cuts through the outflow region.

In Sect. 2 we summarize our observations. In Sect. 3 we present the general method for determining the o/p ratio and the excitation temperature, which we then test with existing wide-beam data. In Sect. 4, we present the ortho-para ratio and excitation distributions for OMC-1 and discuss the implications in Sect. 5.

2. Observation and reduction technique

The images were obtained on 13–15 December 1995, at the ESO/MPI 2.2m telescope at La Silla, Chile, with the IRAC2 infrared camera and the associated Fabry-Pérot interferometer (FP). The IRAC 2 camera is equipped with a 256×256 pixel NICMOS array and was used with optics that yield a 0.52''/pixel scale and a 128''×128'' field of view. The FP is built by Queensgate Instruments Ltd. (serial number ET70WF-923). The etalon has a measured finesse $F \geq 50$, and a transmission of 70%-

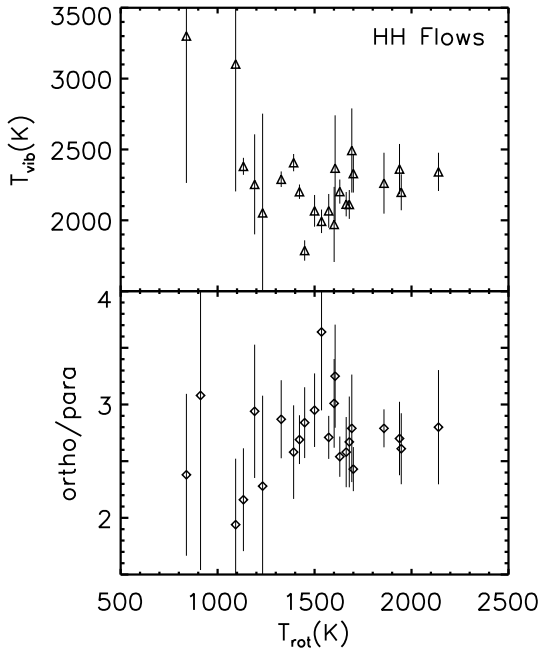


Fig. 1. The ortho-para ratio and excitation temperatures in various Herbig-Haro objects and outflows

80% in the 2.04-2.46 μm wavelength range (measured by Anton van Dijsseldonk, 1992, ESO internal memorandum). The announced resolution is $\frac{\lambda}{\Delta\lambda} \sim 1000$, although we measured it to be closer to 1500 (200 km/s at 2 microns). At each wavelength observed, narrow-band “blocking” filters were used to isolate the orders (see Table 1).

In each of the H_2 lines observed, we imaged OMC-1 with the FP tuned, first to the line rest wavelength, then to a “continuum wavelength” (typically 0.004 - 0.007 μm from the line wavelength, avoiding bright airglow lines; see Table 1), and then to the blue- and red-shifted wings of the FP profile (i.e. roughly $\pm 0.001 \mu\text{m}$, or $\pm 140 \text{ km s}^{-1}$). These images allowed us to check the accuracy of the tuning of the FP: by fitting gaussians to photometric measurements from the line and wing images (calibration frames were obtained for each of the 5 lines observed), we established that the FP does indeed accurately tune to the desired line wavelength.

Once we had “peaked-up” on the line flux in this way, we observed, consecutively, line + continuum source and line + continuum sky frames. Typically, sky frames were obtained every 60-120 secs. The ESO-MIDAS reduction software was used to reduce the data. Each frame was “sky-subtracted” and flat-fielded in the normal way, using the sky frames observed just before or after each object frame, and dome flat fields taken at the end of each night (for the flat-fielding, images of the inside of the telescope dome, illuminated with a halogen lamp, were observed at each FP wavelength setting). Frames were linearized before averaging. The same source that appears in all of our images, IRC9, was used to flux calibrate the data. A black-body fit to the J, H and K magnitudes of this standard (N. Minchen, 1996, priv. comm) was used to predict the flux density at each

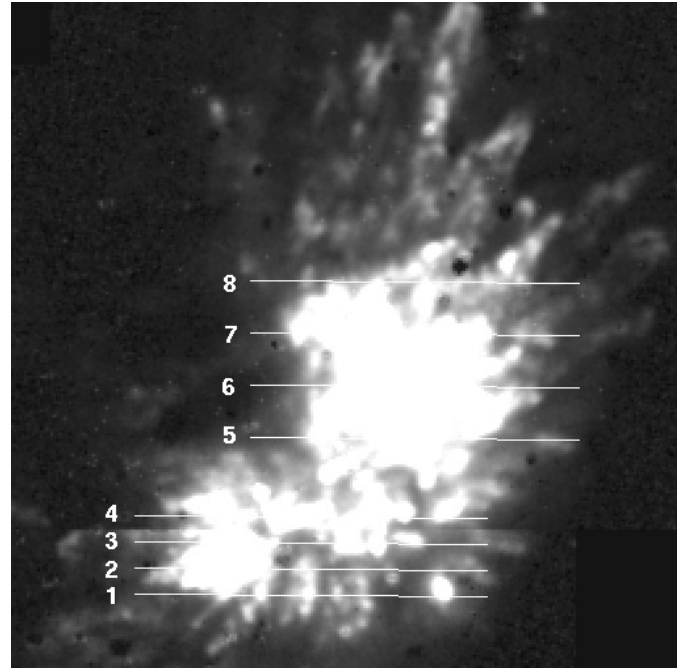


Fig. 2. The 1-0 S(1) map of OMC-1 at 0.52'' resolution with east-west cuts 1-8 running from south (1) to north (8).

wavelength observed: these data were then used to calibrate the response of the system to photons at each wavelength.

Finally, before subtracting continuum frames from line emission frames, the images were smoothed with a 2-D gaussian function so that the mean point-spread-function in each pair of images was as closely matched as possible. Residual artifacts in the differenced images were removed by hand.

3. Extracting the o/p ratio

3.1. Framework

The observations yield three line intensities L_0 , L_1 and L_2 , measured in a beam of fixed solid angle θ^2 . The S(0) and S(2) transitions involve para H_2 with mass fraction $\psi_i = \psi(p)$, and the S(1) transition is ortho with fraction $\psi(o)$, so that $\phi = \psi(o)/\psi(p)$. The energies and rotational quantum numbers of the upper levels of the transitions are $E_i = kT_i$ and J_i . The transition wavelengths are λ_i , radiative de-excitation rates B_i and we assume extinctions A_i . This yields the extinction corrected line fluxes $F_i = 10^{0.4A_i} L_i$. The line fluxes are related to the intrinsic intensities I_i , assuming optically thin isotropic radiation, by $F_i = (\theta^2/4\pi)I_i$.

The intensities are given by

$$I_i = hc \frac{N_i B_i}{\lambda_i} \quad (1)$$

where

$$N_i = \psi_i N(\text{H}_2) \frac{(2J_i + 1) \exp(-T_i/T)}{Z_i(T)} \quad (2)$$

Table 2. The ortho-para ratio (ϕ) and excitation in Herbig-Haro outflows

Source	Location	ϕ	%	T_{rot}	T_{vib}		S(1)/S(0)	S(1)/S(2)	A_K	ref.	
OMC-1	Peak 1	2.95	11	1500	2067	±	112	4.06	3.12	0.87	1
OMC-1	Peak 1	3.01	13	1601	1971	±	265	4.22	3.09	0.87	2
OMC-1	Nebula	2.94	20	1191	2254	±	353	3.72	3.46	0.87	2
OMC-1	Cloud	2.38	30	839	3301	±	1037	2.55	3.50	0.87	2
HH7	Row32	2.87	12	1328	2290	±	55	3.75	3.22	1.00	3
HH7	Row33	2.58	16	1392	2407	±	61	3.43	2.83	1.00	3
HH7	Row34	2.69	8	1422	2202	±	51	3.61	2.93	1.00	3
HH7	Row35	2.16	21	1133	2381	±	60	2.66	2.63	1.00	3
HH7	Pos1	2.54	7	1630	2203	±	85	3.69	2.52	0.46	4
HH7	Pos2	2.58	12	1663	2114	±	86	3.77	2.54	0.46	4
HH7	Pos3	3.25	14	1606	2368	±	373	4.70	3.24	0.46	4
HH7	Pos4	2.43	8	1700	2330	±	134	3.57	2.37	0.46	4
HH7	Pos5	2.71	7	1573	2067	±	119	3.89	2.72	0.46	4
HH7	Pos6	2.61	12	1947	2198	±	127	3.98	2.43	0.46	4
HH10	Pos7A	2.67	15	1679	2112	±	102	3.92	2.60	0.39	4
HH10	Pos7B	2.28	35	1232	2053	±	700	3.02	2.54	0.39	4
HH11	Pos8AB	2.80	18	2139	2342	±	135	4.43	2.46	0.12	4
HH11	Pos8A	2.79	17	1692	2493	±	297	4.16	2.66	0.12	4
HH11	Pos8B	2.70	12	1938	2362	±	177	4.17	2.45	0.12	4
ASR5	Pos9	2.79	6	1858	2262	±	215	4.33	2.55	0.00	4
HH1	Knot A	1.94	30	1093	3103	±	899	2.37	2.37	0.80	5
TTau	NW	2.84	11	1449	1787	±	72	4.07	2.89	0.16	6
TTau	Jet	3.64	19	1536	1993	±	83	5.31	3.61	0.16	6
TTau	Diffuse	3.08	50	912	0	±	0	3.63	4.05	0.16	6

References: ¹ Everett et al (1995), see also Hasegawa et al (1987) ²DePoy & Pogge (1994), ³ Fernandes & Brand (1995), ⁴Everett (1997), ⁵Noriega-Crespo & Garnovich (1995), ⁶Herbst et al (1996)

where $N(\text{H}_2)$ is the total column density, $Z_i(T)$ is the appropriate partition function for ortho or para H_2 and h and c are the standard physical constants. We therefore assume here that the gas is in LTE and at a single temperature T which depends only on position. The LTE assumption is clearly valid for OMC-1, even with vibrational transitions involving the second vibrational level (Brand et al 1988). Here, we employ strong rotational transitions only in the first vibrational level, two factors which ensure LTE.

All the gas observed within a pixel is unlikely to be at the same temperature. Each pointing measures gas with a range of temperatures and it follows that the excitation temperature depends on the upper energy levels of the transitions involved (Brand et al 1988). Note that the excitation temperature T_{ex} is defined between any two upper levels in terms of the column density ratios and generally requires knowledge of the ortho-para ratio. However for the two para transitions we have observed

$$\frac{N_2}{N_0} = \frac{2J_2 + 1}{2J_0 + 1} \exp((T_0 - T_2)/T_{ex}). \quad (3)$$

Note that by plotting $\log N_i$ against T_i , straight lines would denote a constant temperature and convex lines a range in temperatures.

Here, we have chosen three lines which are quite closely spaced in upper energy levels, so we do not expect a large dif-

ference in excitation temperature. We have tested how this assumption will effect the derived values of ϕ using the C-type bow shock which provides an overall fit to the OMC-1 Peak 1 data over a wide range of energy levels (Smith, Brand & Moorhouse 1991a) and with J-type shocks (Smith 1994) which also demonstrate strong $\log N_i - T_i$ curvature. The models presume $\phi = 3$, but yield slightly lower values when we apply the final formula presented below to the 1-0 S(0), S(1) and S(2) transitions. We find $\phi = 2.978$ for the C-type and 2.989 for the J-type model. The fact that these are below 3 is expected since the convex curvature implies that $\log N_1$ will lie below the linear connection between the two neighbouring lines. Thus we conclude that the fixed temperature assumption may introduce an error of at most one per cent. (One means of overcoming this error would be to include a fourth line, the 1-0 S(3), to define the curvature. However, this line lies outside the K-band and cannot be reliably measured from the ground).

The partition functions are the sums of $(2J_i + 1)\exp(-T_i/T)$ over all energy levels. They could be calculated implicitly for each temperature and H_2 form. However, we have calculated the ortho and para partition functions and compared them to a single, straightforward approximation over the excitation temperature interval observed for OMC-1. We find that

$$Z(T) = 6.13510^{-3} T [1 - \exp(-5850/T)]^{-1} \quad (4)$$

is 0.2% accurate over the temperature range 850K - 1900K and remains 1.0% accurate for 600K - 2450K. We thus are able to employ this single partition function for both species below.

3.2. Method

The expression for ϕ which we use is:

$$\phi = \left[\frac{N_1/(2J_1 + 1)}{N_2/(2J_2 + 1)} \right]^{\frac{T_1 - T_0}{T_2 - T_0}} \left[\frac{N_1/(2J_1 + 1)}{N_0/(2J_0 + 1)} \right]^{\frac{T_2 - T_1}{T_2 - T_0}} \quad (5)$$

which is generally valid for any three rotationally-consecutive lines (where $1/\phi$ is derived for sequences containing two ortho transitions). This equation is derived from the expression for the N_2/N_1 ratio (from Eq. (2),

$$\frac{N_2}{N_1} = \frac{1}{\phi} \frac{2J_2 + 1}{2J_1 + 1} \exp((T_1 - T_2)/T_{ex}), \quad (6)$$

on making the substitution

$$\exp \frac{T_1 - T_2}{T_{ex}} = \left[\exp \frac{T_0 - T_2}{T_{ex}} \right]^{\frac{T_1 - T_2}{T_0 - T_2}} \quad (7)$$

and then using Eq. (3) to eliminate T_{ex} .

We therefore only need to derive dereddened columns from the data to extract the ortho and para fractions. The column density ratios are given from Eq. (1) in terms of the observed line strengths:

$$N_j/N_k = \frac{\lambda_j L_j B_k}{\lambda_k L_k B_j} 10^{0.4(A_j - A_k)}. \quad (8)$$

For the three lines chosen here, with $T_i = 6471\text{K}$, 6951K & 7584K , $B_i/10^{-7} = 2.53, 3.47$ & 3.98 this yields

$$\phi = 0.809 \eta \left[\frac{L_1}{L_2} \right]^{0.431} \left[\frac{L_1}{L_0} \right]^{0.569} \quad (9)$$

where

$$\eta = 10^{0.173(A_1 - A_2) + 0.227(A_1 - A_0)}. \quad (10)$$

The extinction dependence is very weak. For example, adopting the extinction curve of Mathis (1990) and the extinction to Peak 1 of OMC-1 of $A_J = 2.15 \pm 0.26$ (Everett, DePoy & Pogge 1995), yields $\eta = 1.0084$. That is, for OMC-1, ignoring extinction altogether introduces on average underestimates of the ortho-to-para ratio of under 1%. Hence, the three lines observed (1-0 S(0), S(1) & S(2)) permit an accurate estimate for ϕ .

The rotational excitation temperature derived from Eq. (3) has a much stronger extinction dependence, however, since

$$T_{ex} = \frac{1113\text{K}}{1.13 + 0.92(A_0 - A_2) + \ln(L_0/L_2)}. \quad (11)$$

which yields a value of $1500\text{K} \pm 146\text{K}$ for OMC-1 Peak 1, as given in Table 2.

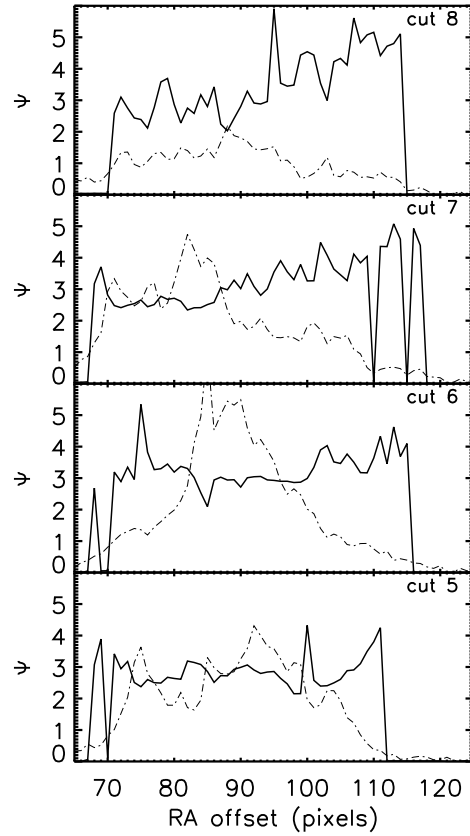


Fig. 3. The ortho-para ratio in the north of OMC-1 for the top four slit positions in Fig. 2. Pixels here are $1.04''$. The broken line is the relative 1-0 S(0) flux.

3.3. General results

The values for ϕ derived from Eq. (7) are listed in Table 2 and plotted in Fig. 1 for a number of Herbig-Haro objects. The extinctions are taken from the corresponding reference. The quoted error is simply the highest error quoted for the three lines involved. This may include calibration as well as continuum subtraction errors. Hence only a crude error analysis is feasible here. Note, however, that ϕ depends at most linearly on each line flux, so the quoted error can be taken as an upper limit. The ortho-para ratio is consistent with 3 in each object in which the errors are less than 25%.

We remark that the contradictory results for HH 7 reported by Fernandes & Brand (1995) and Everett (1996) have been resolved here. The observations are, after all, in agreement (upon removing an error in the conversion of fluxes to columns in the earlier publication). We also note that where the errors are large in Fig. 1, the ratio falls below 3 and the rotational excitation temperature is relatively low. This suggests that the 1-0 S(0) flux has not been accurately measured in these objects. An alternative is that weaker lines are produced in cooler objects where ortho-para conversion is slow, thus revealing the value acquired from post-formation processes in cool surroundings. This is less plausible on theoretical grounds, however, since the

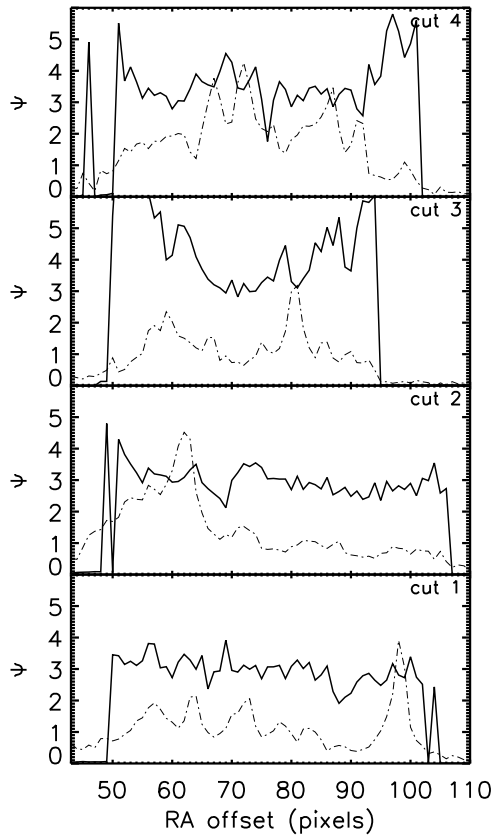


Fig. 4. The ortho-para ratio in the south of OMC-1 for the bottom four slit positions in Fig. 2. Pixels here are $1.04''$. The broken line is the relative 1-0 S(0) flux.

conversion rate coefficients are not particularly sensitive to the temperature in the range 1000K-1600K (Burton et al 1992).

Finally, note that in Table 1 the rotational excitation temperatures are consistently below the vibrational 2-1/1-0 S(1) excitation temperatures. This is expected from shock theory when either hot gas is produced and allowed to cool unhindered (J-type), or when a variety of shock strengths are involved (supersonic turbulence and/or curved shock fronts). The narrow range in vibrational temperature may result from the fixed manner in which warm gas cools as well as the ubiquitous presence of bow-type shock fronts (Smith et al 1991a).

4. The OMC-1 ortho-para distribution

In Fig. 2 we present the OMC-1 1-0 S(1) image. We see the extended bullets very clearly in this image since the line/continuum ratio is enhanced over that measured in normal narrow-band filters (the FP bandpass measures $\Delta\lambda/\lambda \sim 0.1$). In Figs. 3 & 4 we show the ortho-para ratio for several east-west cuts through the source as well as the relative intensity of the 1-0 S(0) line. The rotational temperature corresponding to the E-W cuts is shown in Figs. 5 & 6. Note that no values are derived for pixels in which any individual line flux could not be accurately determined.

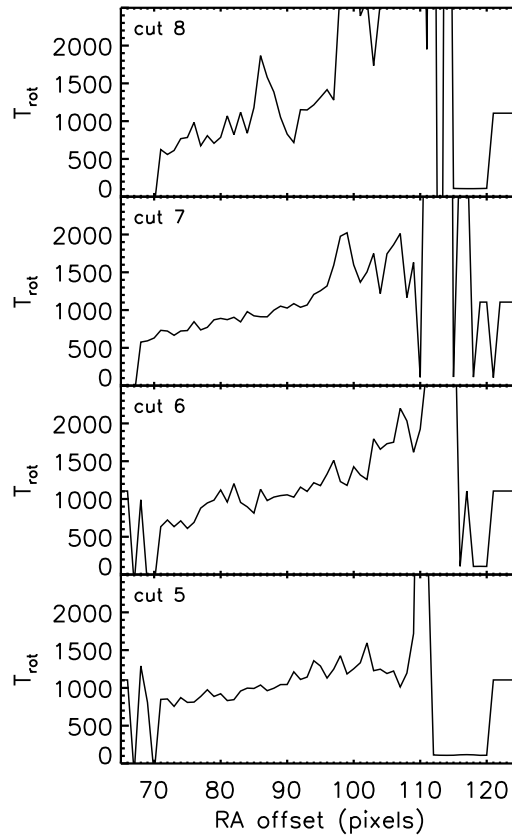


Fig. 5. The rotational temperature in the north of OMC-1 for the top four slit positions in Fig. 2

We find:

- The ortho-para ratio is consistent with 3 in all regions where the 1-0 S(0) line is strong.
- The rotational temperature increases quite monotonically from east to west in the northern lobe. The 1-0 S(1) flux does not show any related variation. Hence a differential extinction effect, in which extinction would dominate the intensity distribution, can be excluded. Temperature variations were found in the southern lobe by Schild et al (1997) from the S(1) and S(2) transitions (with the same instrument), having assumed an ortho-para ratio equal to 3. In the south (see Cuts 1 & 2), we see that the rotational temperature rises steadily from 880K to over 1300K from east to west.
- The increase in the ortho-para ratio above 3 on the western side of the outflow is a sensitivity effect; the 1-0 S(0) emission becomes too weak (as the temperature rises) to be reliably measured. Similarly, the rotational temperature across Cut 3 is highly non-uniform, and the derived ϕ unreliable.

If we were to assume, on theoretical grounds, that $\phi \sim 3$ throughout the lobes, then the measured value of ϕ provides a check on the flux levels. If we find $\phi \sim 3$ in large areas, then we can be assured that any associated temperature variations are not

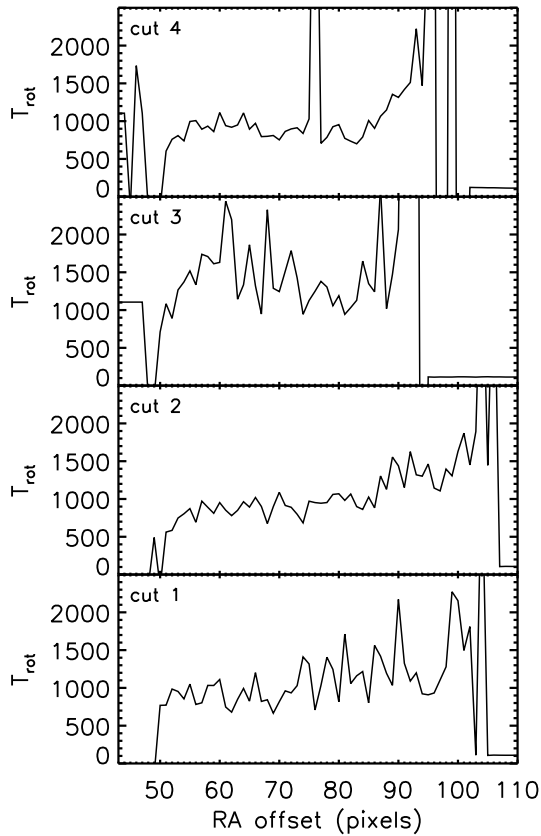


Fig. 6. The rotational temperature in the south of OMC-1 at 1'' resolution for the bottom four slit positions in Fig. 2

due to badly-measured line fluxes but actually require a physical explanation. In the above findings, it thus seems unlikely that ϕ really exceeds 3, supporting the interpretation that the 1-0 S(0) flux is not fully measured when the temperature is high.

We present the vibrational temperature T_{vib} in Figs. 7 & 8. The 2-1 S(1) and the 2-1 S(3) (see Fig. 9), have not been so accurately measured. Nevertheless, it is remarkable how constant T_{vib} remains through some of the cuts (e.g. 7 & 8) even though the rotational temperature rises steadily in the same region.

5. Implications

The graphical method to determine ϕ proceeds by assuming the value of 3, plotting column density against upper energy level, and then inspecting for systematic offsets between the para and ortho lines. For example, Wright et al (1996) have recently applied this method to ISO data for Cepheus A, finding no measurable offset. To find a *distribution* in ϕ , however, requires an analytical method such as developed here. This method yields ortho/para ratios consistent with 3 in various HH objects as well as across the OMC-1 outflow.

Why are no variations in ϕ detected? Either the molecules formed in a warm state ($T > 200$ K) according to the statistical weights, or the molecule fractions have been altered to this value within the gas phase. H_2 formation is most efficient

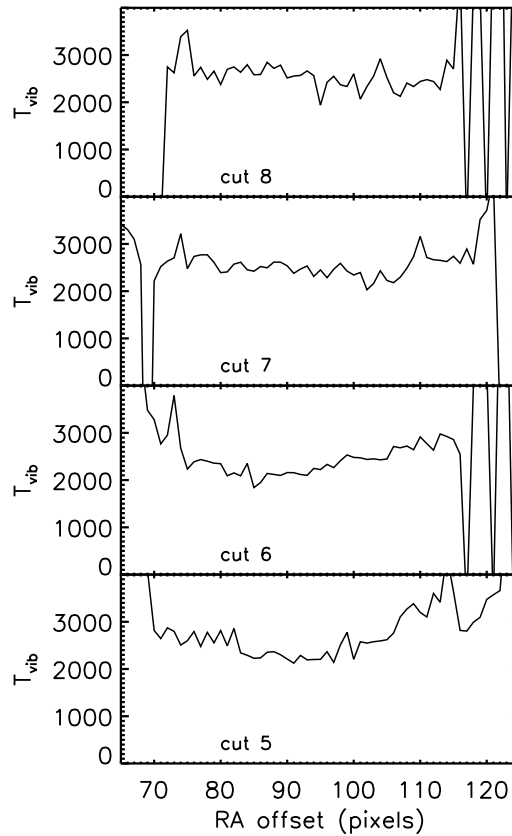


Fig. 7. The vibrational temperature derived from the 1-0 S(1) and 2-1 S(1) fluxes in the north of OMC-1 for the top four slit positions in Fig. 2

on dust in a dense environment with a formation rate of order $3 \cdot 10^{-17} n(H) s^{-1}$, or a formation timescale of $10^5/n_4$ years where $n_4 = n(H)/(10^4 cm^{-3})$ (see Duley 1996). The formation is expected to yield a value of 3.

The H_2 can be converted before leaving the grain or later, on colliding with a grain. The conversion rate is then of order of the H_2 formation rate (Burton et al) and thus produces strong reductions from the statistical weights, $\phi = 3$, in cool quiescent molecular clouds. This is a satisfactory explanation for the low ϕ values in photon dominated regions such as NGC 2023 where $\phi \sim 1.7 \pm 0.3$ (Hasegawa et al 1987). This mechanism could also, however, be expected to lower ϕ wherever the H_2 has formed. A secondary warm thermalisation process appears necessary.

Reactions with protons would transform ortho and para, producing thermal equilibrium between the modifications on a timescale of $30/n(H^+)$ years (Dalgarno et al 1973, Flower & Watt 1984). The predicted very low proton densities in cold clouds e.g. $n(H^+) = 10^{-5} cm^{-3}$ (Flower & Watt 1984) generally imply this to be an inefficient conversion mechanism, consistent with the observed ϕ values. On the other hand, numerous warm shocks or regions of supersonic turbulent dissipation within bipolar outflows could provide the necessary column of

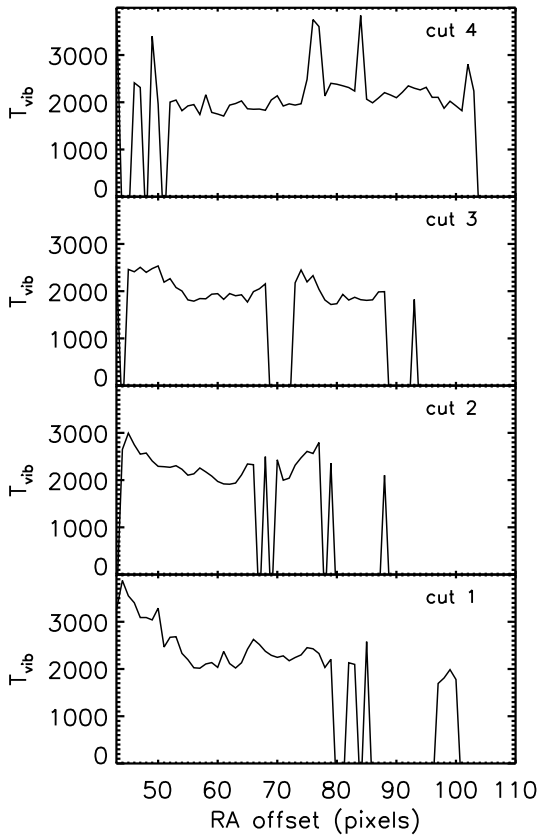


Fig. 8. The vibrational temperature derived from the 1-0 S(1) and 2-1 S(1) fluxes in the south of OMC-1 for the bottom four slit positions in Fig. 2

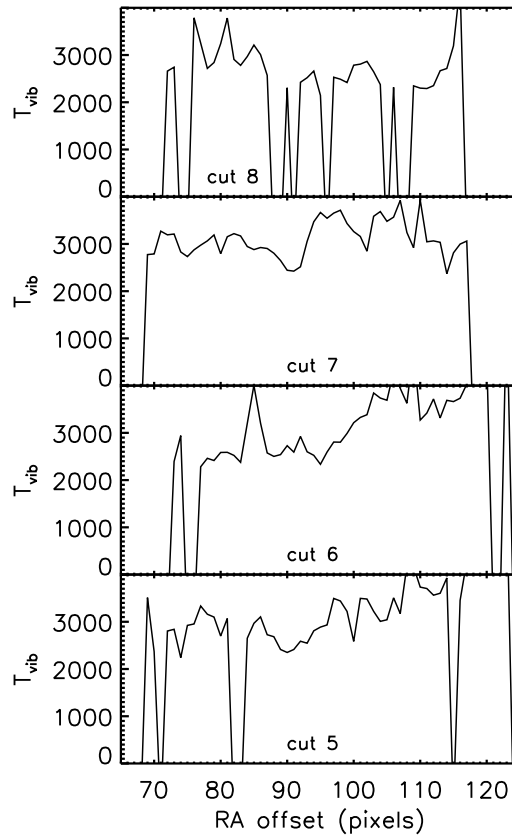


Fig. 9. The vibrational temperature derived from the 1-0 S(1) and 2-1 S(3) fluxes in the north of OMC-1 for the top four slit positions in Fig. 2. The data for the south cuts, of low quality, are not shown.

protons to convert ϕ to the value of 3. Detailed calculations need to be performed.

Atomic H can induce ortho-para conversion when the gas is warm, with an estimated rate of $1.6 \times 10^{-11} \exp(-3200K/T) \phi n(H) s^{-1}$ (Burton et al 1992, see also Martin et al 1996). The activation barrier and the need for significant atomic H makes this process important in the shocks themselves. Furthermore, atomic H can be large in 'molecular' hydrodynamic shocks as well as in jet-driven outflows (Suttner et al 1997). Given a cooling time for the vibrationally-excited H_2 gas of order of 1 year, then the thermal equilibrium value at high temperatures and densities, $\phi = 3$, will be generated in the shocks themselves for $n(H)$ above $\sim 10^4 \text{ cm}^{-3}$.

Such high atomic densities would be convenient for shock modellers for another reason: to generate LTE (as clearly observed in OMC-1). Local thermodynamic equilibrium is difficult to produce through H_2 - H_2 collisions alone, unless high densities are admitted ($n(H_2) \gg 10^6 \text{ cm}^{-3}$). Richter, Graham & Wright (1995) solved this possible problem by proposing that atomic H is the major collision partner. Present collision rates imply that atomic H dominates when present at a level of just a few per cent. This, however, as well as the ortho-para rate, remains to be confirmed through rigorous quantum calculations.

Acknowledgements. This work was supported by the Deutsche Forschungsgemeinschaft through the Schwerpunkt Programm 'Physics of Star Formation' (grant Zi-242/10-1).

References

- Allen D. A. & Burton M. G., 1993, *Nature*, 363, 54
- Axon, D. A. & Taylor, K. N. R. 1984, *MNRAS*, 207, 241
- Beckwith S., Persson S. E., Neugebauer G. & Becklin E., 1978, *ApJ*, 223, 464
- Black, J., van Dishoeck, E., 1987, *ApJ*, 322, 412
- Brand, P. W. J. L., Moorhouse, A., Burton, M. G., Geballe, T. R., Bird, M., & Wade, R. 1988, *APJL*, 334, L103
- Brand, P. W. J. L., Toner, M. P., Geballe, T. R., Webster, A. S., Williams, P. M., & Burton, M. G. 1989a, *MNRAS*, 236, 929
- Brand, P. W. J. L., Toner, M. P., Geballe, T. R., Webster, A. S., Williams, P. M., & Burton, M. G. 1989b, *MNRAS*, 237, 1009
- Burton, M. G., Hollenbach, D. J., Tielens, A. G. G. M., 1992, *ApJ*, 399, 563
- Davis C. J. & Smith M.D., 1995, *ApJL*, 443, L41
- Davis C. J. & Smith M.D., 1996, 310, 961
- Dalgarno, A., Black, J., Weisheit, J., 1973, *Astrophys. Lett.*, 14, 77.
- DePoy, D.L., Pogge, R.W., 1994, *ApJ*, 433, 725
- Draine, B. T. & McKee, C. F. 1993, *ARA&A*, 31, 373
- Duley, W.W., 1996, *MNRAS* 279, 591
- Eisloffel, J., Smith, M.D., Davis, C.J., Ray, T.P., 1996, *AJ*, 112, 2086

- Everett, M. E., DePoy, D. L., & Pogge, R. W. 1995, *AJ*, 110, 1295
- Everett, M. E., 1997, *ApJ*, 478, 246.
- Fernandes, A.J.L., Brand, P.W.J.L., 1995, *MNRAS*, 274, 639
- Flower, D.R., Watt, G.D., 1984, *MNRAS*, 209, 25
- Genzel, R. & Stutzki, J. 1989, *ARA&A*, 27, 41
- Liseau, R., et al, 1996, 315, 181L.
- Hasegawa, T., et al, 1987, *ApJL*, 318, L77
- Herbst, T. M., et al, 1996, *AJ*, 111, 2403.
- Martin, P.G., Schwarz, D.H., Mandy, M.E., 1996, *ApJ*, 461, 265
- McCaughrean, M., Mac Low, M.-M., 1997, *AJ*, 113, 391
- Moorhouse A., Brand P. W., Geballe T. R. & Burton M. G., 1990, *MNRAS*, 242, 88
- Noriega-Crespo, A., Garnovich, P.M., 1995, *Ap&SS*, 233, 63
- Richter, M.J., Graham, J.R., Wright, G.S., 1995, *ApJ*, 454, 277
- Schild, H., Miller, S., & Tennyson, J. 1997, *A&A*, 318, 608
- Ramsay, S.K., Chrysostomou, A., Geballe, T.R., Brand, P.W.J.L., Mountain, M., 1993, *MNRAS*, 263, 695
- Smith, M.D. 1991, *MNRAS*, 253, 175
- Smith, M.D. 1994, *A&A*, 289, 256
- Smith, M. D., Brand, P. W., & Moorhouse, A., 1991a, *MNRAS* 248, 451
- Smith, M. D., Brand, P. W., & Moorhouse, A., 1991b, *MNRAS* 248, 730
- Stone J. M., Xu J. & Mundy L. G., 1995, *Nature*, 377, 315
- Sugai H. Usuda T., Kataza H. et al., 1994, *ApJ*, 420, 746
- Sugai H. Kawabata H., Usuda T., et al., 1995, *ApJ*, 442, 674
- Suttner, G., Smith, M.D., Yorke, H.W., Zinnecker, H., 1997, *A&A*, 318, 595.
- Tedds, J. et al. 1995. In *Proc Circumstellar matter*, eds. Watt, G.D., Williams, P.M. (Kluwer).
- Wright, C. et al 1996, *A&A*, 315, L301